Chem. Res. Chinese Universities, 2020, 36(4), 715—720 doi: 10.1007/s40242-020-0149-4

Article

Porous $NiCo_2O_4$ Nanowire Arrays as Supercapacitor Electrode Materials with Extremely High Cycling Stability

CHEN Chaoxian, ZHAO Chenyang, LI Cuihua, LIU Jianhong and GUI Dayong*

College of Chemistry and Environmental Engineering, Shenzhen University, Shenzhen 518055, P. R. China

Abstract In this work, $NiCo_2O_4$(NCO) was synthesized *via* microwave hydrothermal method and a further annealing treatment. Research results have shown that the surface defects(Co^{2+} site) and pore size of the materials can be adjusted by simply changing the calcination temperatures, and porous nanowire arrays structure can be obtained. The porous structure is conducive to the penetration of the electrolyte and enables the NCO to fully participate in the electrochemical reaction. What's more, the NCO material has ample space to buffer the volume change in the cycle test, improving the cycling stability. The NCO obtained at 350 °C has better performance. It exhibits a specific capacitance of 648.69 F/g at 1 A/g and good rate capability. Especially, at 10 A/g, the specific capacitance can still be maintained at 80.00% after 10000 galvanostatic charge/discharge(GCD) cycles, showing excellent cycling stability.

Keywords $NiCo_2O_4$; Porous nanowire array; High cycling stability; Supercapacitor

1 Introduction

With the rapid development of economy, the pressure in the supply of energy has been remarkably increased. In order to alleviate the pressure of energy, researchers have done a lot of work to develop and study new electrochemical energy conversion and storage devices. Among them, supercapacitors(SCs) have caused extensive research because of their advantages, such as fast charge and discharge rates, high power densities, long cycle lifes, and environmental protection[1—3]. Although the energy density of SCs is much larger than that of traditional capacitors, it is still far from that of secondary batteries. Currently, supercapacitors are used with batteries to provide additional power in many applications[4,5]. Combined with other energy devices, they are expected to have a broader application prospects in the field of energy storage.

The electrode materials are a key factor in determining the performances of SCs. Carbon materials have been widely used as electric double layer electrode materials. However, their specific capacitances and energy densities are low[6,7]. Some transition metal oxides, such as MnO_2, TiO_2 and NiO have been extensively studied due to their rich resources, low price, and environmental friendliness. They store charge through the Faraday redox reactions, and their capacitances are much larger than that of carbon materials[8—10]. In recent years, transition binary metal oxides materials, such as $NiCo_2O_4$, $CoMn_2O_4$, $CoFe_2O_4$ and $NiFe_2O_4$ have drawn much attention[11]. On the one hand, both metal components in the bimetallic oxides can undergo redox reactions, and many intermediate valence ions are generated in the electrochemical reactions to store and transfer more charge, which can increase the specific capacitances of the materials, and their theoretical specific capacitances are very high[12]. On the other hand, the electrical conductivity of the binary metal oxides are at least two orders of magnitude higher than that of mono-metal oxides, which can make up for the shortcomings of poor rate capability and cycling stability of mono-metal oxides[13]. Especially for the nickel-cobalt bimetallic oxide, Co has a higher conductivity to reduce the charge transfer resistance and improve the stability of the compound, while Ni can promote the electrochemical activity of the material, increasing the specific capacity and rate performance[14,15].

Although nickel-cobalt bimetallic oxides have outstanding electrochemical performances, they also face some problems. During fast charge and discharge process, the low utilization rates of material result in a low performance rate[11,12]. The nanoporous structures and arrays structures(such as nanotubes, nanowires, and nanorods) can be prepared to solve the above problems. Because the porous and arrayed structures can shorten the transmission distance of ions and electrons, the speed of electrochemical reactions can be accelerated[16—18]. For example, Zhang *et al.*[19] prepared ultrathin $NiCo_2S_4$ nanoflake arrays on nickel foam that displayed a specific capacitance of 1051 F/g at 0.5 A/g and high capacitance retention of 85% at 5 A/g after 5000 cycles. Sethi *et al.*[20] reported $NiCo_2O_4$ nanorod arrays with a specific capacitance of 440 F/g at 5 mV/s and good cyclic stability(94% after 2000 cycles at 8 A/g). Zhang *et al.*[21] fabricated porous $NiCo_2O_4$ nanowire arrays supported on carbon cloth(CC). The $NiCo_2O_4$@CC shows a high specific capacitance of 1183 mF/cm^2 at 1 mA/cm^2 and excellent cyclic stability(a retention rate of 90.4% after 3000 cycles at a current density of 5 mA/cm^2). The excellent

*Corresponding author. Email: dygui@szu.edu.cn

Received May 4, 2020; accepted June 30, 2020.

Supported by the Natural Science Foundation of Guangdong Province, China(No.2017A030313322) and the Project of the Huizhou Ledman Optoelectronic Technology Co., Ltd., China(No.17006157).

electrochemical behaviors could be attributed to the porous nanowire arrays characteristics of $NiCo_2O_4$, which shortens the transportation channels of ions to promote electrochemical reactions during rapid redox reaction process. In addition, $NiCo_2O_4$ was directly grown on conductive CC, avoiding the addition of the binder and promoting a rapid transport of ion and electron, thus the electrochemical performances are enhanced.

In this study, $NiCo_2O_4$(NCO) with porous nanowire arrays structure was synthesized *via* one-step microwave hydrothermal method and a further annealing treatment. And a series of $NiCo_2O_4$ electrode materials was obtained by post-calcination under different temperature conditions. The study found that the surface defects(Co^{2+} site) and nanopore size of the materials can be effectively controlled by changing the calcination temperature. The resulting NCO at 350 °C(NCO-350) has a higher specific capacitance and cycling stability. It exhibits a specific capacitance of 648.69 F/g at 1 A/g and good rate capability(66.80% retention of initial capacitance from 1 A/g to 20 A/g). Above all, its specific capacitance can still be maintained at 80.00% at 10 A/g after 10000 galvanostatic charge/discharge(GCD) cycles. The above behaviors imply the potential practical applications of the NCO-350.

2 Experimental

2.1 Chemicals

Cobalt chloride hexahydrate($CoCl_2·6H_2O$) and nickel chloride hexahydrate($NiCl_2·6H_2O$) were purchased from Shanghai Macklin Biochemical Co., Ltd.(Shanghai, China). Urea[$CO(NH_2)_2$] was obtained from Tianjin Zhiyuan Chemical Reagent Co., Ltd.(Tianjin, China). All chemicals were used as received.

2.2 Synthesis of the Ni-Co Precursor

For the synthesis of the precursor, 1 mmol of $NiCl_2·6H_2O$, 2 mmol of $CoCl_2·6H_2O$ and 10 mmol of urea were dissolved into 60 mL of deionized water to form a transparent pink solution by vigorously stirring for 30 min. Then the mixture was transferred into a 100 mL microwave hydrothermal container(XH-8000Plus, Beijing Xianghu Science and Technology Development Co., Ltd, China), and maintained at 150 °C for 4 min with vigorous and continuous stirring. After cooling to room temperature naturally, the precursor was washed with distilled water and ethanol several times, and vacuum dried at 75 °C for 12 h. Finally, a blue-purple Ni-Co carbonate hydroxide precursor powder was obtained.

2.3 Synthesis of the NCO

In a typical synthesis of the NCO-350, a certain quality of the above-mentioned blue-violet precursor powder was annealed in a muffle furnace, heating to 350 °C with a rate of 2 °C/min and keeping for 2 h. After the temperature dropped to room temperature, NCO-350 black powder was obtained.

For comparison, the basic procedure was the same as that stated above, but the calcination temperature was changed to 300, 400 or 450 °C, respectively. The resulting samples were labeled as NCO-300, NCO-400 and NCO-450.

2.4 Materials Characterization

The crystal phase and chemical state of the products were characterized by X-ray powder diffraction(XRD, Empyrean, Netherlands) with a Cu *Kα* radiation operating at 60 kV, 100 mA and X-ray photoelectron spectroscopy(XPS, K-Alpha+, UK) spectra. The morphology and microstructure were characterized on a field-emission scanning electron microscope (FESEM, JSM-7800F & TEAM Octane Plus, Japan) equipped with an X-ray energy-dispersive spectroscopy(EDS) system, and a transmission electron microscope(TEM, JEM-2100 & X-Max80, Japan).

2.5 Electrochemical Characterization

The working electrodes were prepared using homogeneous slurry of NCo_2O_4, acetylene black, and polyvinylidene fluoride binder with a mass ratio of 8:1:1 in *N*-methyl-2-pyrrolidone. The prepared slurry was then coated on the pretreated Ni foam(NF, 14 mm diameter, 1.5 mm thickness, 99.8%) substrate and dried at 60 °C in vacuum for 12 h. The typical mass loading of active material was around 2.0 mg. In order to investigate the electrochemical performance of the as-prepared NCO electrodes, the electrochemical tests including cyclic voltammetry(CV), GCD and electrochemical impedance spectroscopy(EIS) were conducted on a CHI 760E electrochemical workstation(Chenhua, Shanghai) in 6 mol/L KOH aqueous electrolyte with a three electrode system, in which platinum plate electrode and Hg/HgO electrode were used as counter and reference electrodes, respectively. The cycling stability test was performed on the LAND battery test system(CT 2001A), that is, the GCD was repeated at a constant current density and the test was repeated thousands of cycles.

The specific capacitance(C_s, F/g) of the NCO for three electrode methods from GCD data was calculated according to the following equation[22,23]:

$$C_s=I\Delta t/m\Delta V \quad (1)$$

where I is the discharge current(A), Δt is the discharge time(s), m is the mass of active material(g) and ΔV is the discharge potential range(V).

3 Results and Discussion

3.1 Structural and Morphological Characterization

To analyze the crystal structure and purity of the synthesized NCO materials, XRD analysis was carried out and the results are exhibited in Fig.1(A). By comparison, it can be found that the diffraction peaks of all NCO samples at 18.9°, 31.1°, 36.7°, 44.6°, 59.1° and 64.9° correspond to the (111), (220), (311), (400), (511) and (440) crystal planes of the standard $NiCo_2O_4$(PDF Card No:20-0781)[24], indicating that $NiCo_2O_4$ was successfully synthesized at different calcination temperatures. At the same time, with the increase of the calcination temperature, diffraction peaks belonging to the NCO

become sharper as well as the intensity increases, which demonstates the crystallinities are enhanced, the defects decrease and the material become brittle accordingly[25]. In addition, no other crystalline phases or obvious impurity peaks are detected, indicating the formation of high-quality $NiCo_2O_4$.

To further understand the near-surface elemental compositions and chemical valence states of the synthesized NCO-350, XPS were measured. As shown in Fig.1(B), two spin-orbit doublets and two shake-up satellites(indicated as "Sat.") can be observed in the Ni_{2p} fine spectrum. In detail, the peaks of binding energies at approximately 872.2 and 854.3 eV are geared to $2p_{1/2}$ and $2p_{3/2}$ of Ni^{3+}, respectively, while 870.6 and 853.1 eV correspond to the peak positions $2p_{1/2}$ and $2p_{3/2}$ of Ni^{2+}. The two peaks situated at 878.6 and 860.3 eV can be regarded as satellites[26]. Similarly, there are also two spin-orbit doublets in the Co_{2p} spectrum[Fig.1(C)]. The peaks at 794.7 and 779.7 eV are ascribed to Co^{2+}, the peaks at 793.6 and 778.4 eV are Co^{3+} peak positions, while the peaks at 801.8 and 782.7 eV are two satellites peaks[27]. The peak area ratios of Ni_{2p}, Co_{2p} and O_{1s} calculated with XPS data are shown in Table S1(see the Electronic Supplementary Material of this paper). It can be found that the relative intensities of Co^{2+} and Co^{3+} differ greatly, and most of the cobalt atoms in the crystal lattice exist as Co^{2+} cations, which is believed to contribute to the improvement in faradaic reactions[25,28,29]. In addition, O_{1s} energy spectrum[Fig.1(D)] can confirm the existence of oxygen vacancies in NCO samples. It can be split into three sub-peaks: the peak position at 528.3 eV(O I) is a typical metal-oxygen bond, the peak at 531.2 eV(O II) is related to the defect site with low oxygen coordination, which indicates the creation of a large amount of oxygen vacancies(58.0%) after the treatment. The introduction of oxygen vacancies(Co^{2+} sites) increases the donor density to enhance the conductivity of the NCO sample, which is conducive to the rapid storage of charge. While, the peak at 531.8 eV(O III) attributes to the water absorbed near the surface[28,30,31]. The above results show that the surface of the prepared NCO-350 contains mixed compositions, including Ni^{2+}, Ni^{3+}, Co^{2+} and Co^{3+}.

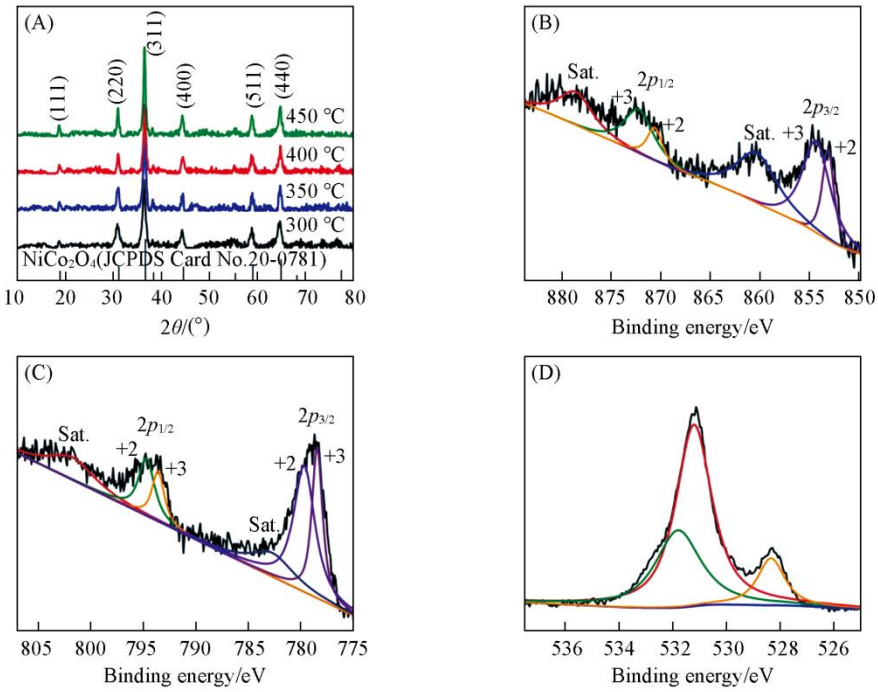

Fig.1 XRD patterns of NCO prepared at different calcination temperatures(A), high-resolution XPS spectra of Ni_{2p}(B), Co_{2p}(C) and O_{1s}(D) of NCO-350

The surface morphologies of the synthesized NCO samples were investigated by FESEM. The nickel-cobalt hydroxide precursor has a nanowire arrays structure with a smooth surface, as observed in Fig.2(A) and (B). As can be seen from Fig.2(C)—(F), after calcination, the four samples have a similar nanowire structure with an open top(diameter approximately 100—300 nm), and the surface is roughened by plentiful pores. And the surface became rougher and the pore became larger with the increasing calcination temperature.

The formation of the porous structure is obtained from the thermal decomposition or oxidation of the precursor after calcination process, and the gas is continuously released from the precursor. The porous nanowire arrays structure is conducive to the penetration of electrolyte ions from the outside to the inside of the material, promoting the migration of electrolyte ions, thereby improving the utilization of electrode materials. Moreover, the porous structure makes the material have plenty of space to buffer the volume changes during the high current density cycle test, improving the cycling stability of the material[32,33].

The morphology and crystallinity of the NCO-350 sample were further characterized by TEM. Fig.3(A) shows a single nanowire. Obviously, it can be seen that there are pores between the grains, which is in good agreement with the SEM observation. HRTEM image depicted in Fig.3(B) reveals that the lattice spacing is about 0.28 nm, which corresponds to the (220) lattice plane of $NiCo_2O_4$[34], which is consistent with the previous XRD analysis results.

The N_2 adsorption/desorption isotherms of the NCO-350 are shown in Fig.S1(see the Electronic Supplementary Material

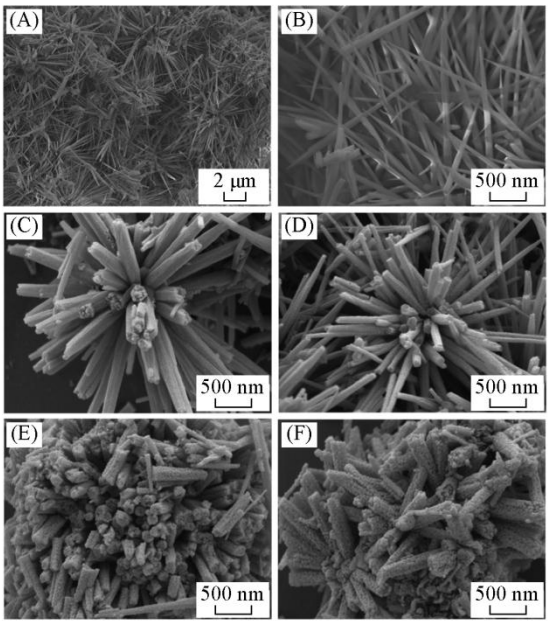

Fig.2 FESEM images of Ni-Co precursor(A, B), NCO-300(C), NCO-350(D), NCO-400(E) and NCO-450(F)

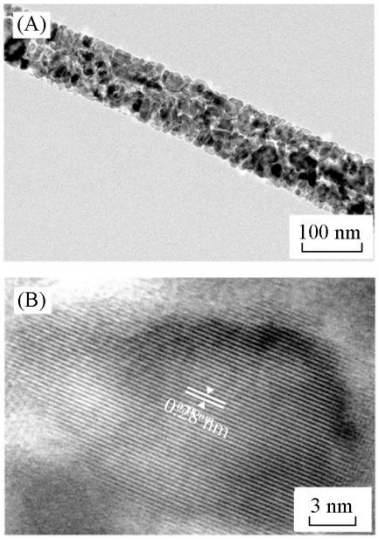

Fig.3 TEM(A) and HRTEM images(B) of NCO-350

of this paper). The Brunauer-Emmett-Teller(BET) surface area is 81.5 m^2/g. Obvious, hysteresis loop can be observed in the range of 0.7—1.0 p/p_0[Fig.S1(A)], which indicates NCO-350 sample has a mesoporous structure. The pore size distribution of the sample calculated desorption isotherm by the Barret-Joyner-Halenda(BJH) can also be seen in Fig.S1. The NCO-350 has sharp peaks at around 3.15, 3.95, 5.08 and 9.97 nm[Fig.S1(B)], the average pore diameter is 5.54 nm and the pore volume is calculated to be 0.11 cm^3/g. The above results predict that the NCO-350 will have impressive electrochemical performance, and further characterization is performed to prove this hypothesis.

3.2 Electrochemical Performances of NCO

To compare the electrochemical performances of NCO products obtained at different calcination temperatures, the CV, GCD, EIS and cycling stability test were carried out with 6 mol/L KOH electrolyte. Fig.4(A) shows the representative CV curves of the four samples at a scan rate of 5 mV/s in a potential window of 0.0—0.6 V(*vs.* Hg/HgO). Each curve shows a pair of well-defined redox peak, which can be attributed to the valence transformations between Ni^{2+}/Ni^{3+}, Co^{2+}/Co^{3+} and Co^{3+}/Co^{4+} and generate NiOOH, CoOOH and CoO_2, indicating the Faradic capacitance characteristics[35,36]. It is found that the area of the CV curve of NCO prepared at 350 °C is slightly larger, showing that NCO-350 has a larger specific capacitance.

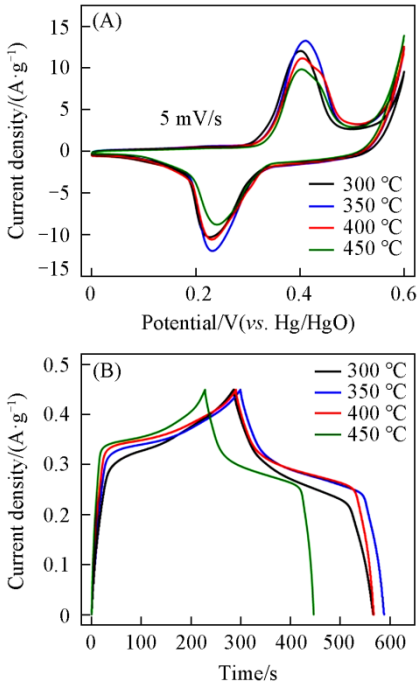

Fig.4 CV curves at 5 mV/s between 0 and 0.6 V(A) and GCD curves at 1 A/g(B) of NCO obtained at different calcination temperatures

Fig.4(B) is GCD curves of four samples at a current density of 1 A/g. Obviously, the GCD curves are nonlinear and have obvious platforms, implying the Faraday capacitance behavior, which is consistent with the CV curves. According to the data of GCD curves, combining with equation (1), the specific capacitances of the NCO can be calculated. At a current density of 1 A/g, the specific capacitances of NCO-300, NCO-350, NCO-400 and NCO-450 are 628.85, 648.69, 621.61, and 491.31 F/g, respectively, which further prove that NCO-350 has a higher specific capacitance.

Fig.5(A) shows the CV curves of NCO-350 at different scan rates. With the scan rates increasing from 5 mV/s to 30 mV/s, the corresponding redox peak will shift. That is, the anode and cathode peaks gradually move to the positive and the negative electrodes, respectively, resulting in an increase in the potential difference between the oxidation and reduction peaks. This is mainly because that the internal resistance of the electrode material increases and polarization occurs at high scan rates[37,38]. However, the shapes of CV curves do not significantly change at different scan rates, indicating that the redox reaction of the sample is still rapid and reversible. As shown in Fig.5(B), all GCD curves have obvious charge and discharge platforms as the current density increases from 1 A/g to 20 A/g,

indicating the good reversibility of the redox reactions. The specific capacitances are 648.69, 605.13, 563.17, 533.17 and 433.33 F/g at the current densities of 1, 2, 5, 10 and 20 A/g, respectively.

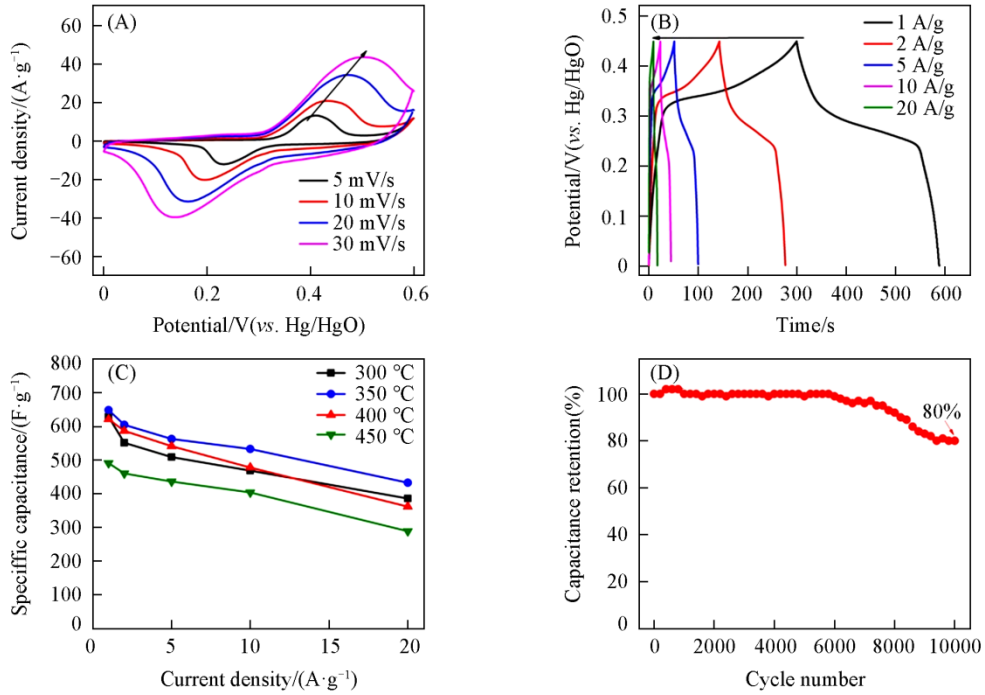

Fig.5 CV curves at different scan rates(A) and GCD curves at different current densities(B) of NCO-350, specific capacitance as a function of current density of samples prepared at different calcination temperatures(C), cycling stability at 10 A/g of NCO-350(D)

Fig.5(C) shows the relationship between the specific capacitances and the current densities of the four NCO samples prepared at different temperatures. It can be seen that as the current density increases, the specific capacitances will decrease. This may be due to that the speed of transmission OH^- to the electrode-electrolyte interface is not fast enough at the high current density[28]. The specific capacitance retention rates of NCO-300, NCO-350, NCO-400 and NCO-450 electrodes are 61.43%, 66.80%, 58.27% and 58.92% from 1 A/g to 20 A/g, respectively, and the NCO-350 sample has a higher rate performance.

Cycling performance is an important parameter of supercapacitors, which can limit their applicability in many applications. As can be seen Fig.5(D), the cycling stability of NCO-350 material is very stable at the first 6000 cycles, and still has 80.00% retention of initial discharge capacity after 10000 cycles, demonstrating that the NCO-350 has a excellent cycling stability. This may be due to that the appropriate oxygen vacancies in the NCO-350 material can enhance the adsorption capacity of OH^- and accelerate the rate of oxidation-reduction reaction. However, the higher temperature treatments will re-oxidize part of Co^{2+} to Co^{3+}, and the oxygen vacancies(Co^{2+} sites) will decrease. Besides, the porous structures make the material have ample space to buffer the volume changes during the a high current density cycle test. Thus, NCO-350 has a better performance than NCO prepared at other calcination temperatures, which is competitive or higher compared to the previous reported results(Table S2[41,42], see the Electronic Supplementary Material of this paper).

As we all know, the electrochemical performance is largely related to the process of ions and charge diffusion, so the electrochemical impedance test was performed in the range of 10^5—0.01 Hz. It mainly includes inherent resistance(R_s), interface charge transfer resistance(R_{ct}) and diffusion resistance(W)[29,39]. As shown in Fig.6, the axis intercepts values of all the NCO electrodes are almost equal in the high-frequency range, but still have a few differences. In other words, the values of R_s increase with the calcination temperatures increase. The R_{ct} corresponds to the size of the semicircle diameter. It is found that the semicircle diameter of NCO-350 is slightly smaller, indicating that it has a better charge transfer performance. In addition, the slopes of the four NCO samples in the low frequency region are relatively close and are similar to the vertical lines, showing that the W values are very small, so that the NCO samples can effectively store charge. But it should be noted that W is not a decisive factor. Therefore, NCO-350 has better conductivity, higher specific capacitance, and better

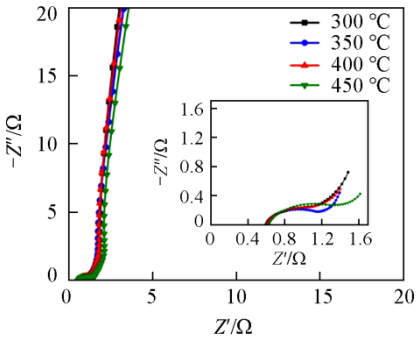

Fig.6 EIS curves of the NCO samples

The inset shows the Nyquist plots at high-frequency region.

cycling performance, proving that it is more suitable for high-performance supercapacitor applications.

4 Conclusions

In summary, $NiCo_2O_4$ materials with porous nanowire arrays structure were successfully synthesized *via* a microwave assisted hydrothermal method and a further calcination process. The surface defects(Co^{2+} site) and pore size of NCO can be adjusted by simply changing calcination temperatures. The introduction of oxygen vacancies can enhance the conductivity of the NCO sample. And the porous nanowire arrays structure allows internal material to expose to the electrolyte, promoting the migration of electrolyte ions. Meanwhile, the structure leaves a large number of pores to buffer the volume change during the cycle test, improving the cycling stability of NCO material. The results show that NCO-350 material has a better electrochemical performance. It exhibits a specific capacitance of 648.69 F/g at 1 A/g and good rate capability(66.80% retention of initial capacitance from 1 A/g to 20 A/g). Especially, at 10 A/g, the specific capacitance can still be maintained at 80.00% after 10000 GCD cycles, showing excellent cycling stability. The above results prove NCO-350 is more suitable for high-performance supercapacitor applications.

Electronic Supplementary Material

Supplementary material is available in the online version of this article at http://dx.doi.org/10.1007/s40242-020-0149-4.

References

[1] Shanmugavani A., Selvan R. K., *Electrochimica Acta*, **2016**, *189*, 283

[2] Zheng Y., Tian Y., Liu S., Tan X., Wang S., Guo Q., Luo J., Li Z., *Journal of Alloys and Compounds*, **2019**, *806*, 170

[3] Conway B. E., *Journal of Electrochemical Society*, **1991**, *138*, 1539

[4] Zhang Y., Yu S., Lou G., Shen Y., Chen H., Shen Z., Zhao S., Zhang J., Chai S., Zou Q., *Journal of Materials Science*, **2017**, *52*, 11201

[5] Shang P., Zhang J., Tang W., Xu Q., Guo S., *Advanced Functional Materials*, **2016**, *26*, 7766

[6] Li Z., Xu K., Pan Y., *Nanotechnology Reviews*, **2019**, *8*, 35

[7] Yu G., Xie X., Pan L., Bao Z., Cui Y., *Nano Energy*, **2013**, *2*, 213

[8] Li W., Xu K., An L., Jiang F., Zhou X., Yang J., Chen Z., Zou R., Hu J., *Journal of Materials Chemistry A*, **2014**, *2*, 1443

[9] Lu X., Wang G., Zhai T., Yu M., Gan J., Tong Y., Li Y., *Nano Letter*, **2012**, *12*, 1690

[10] Vijayakumar S., Nagamuthu S., Muralidharan G., *Applied Materials & Interfaces*, **2013**, *5*, 2188

[11] Li Y., Han X., Yi T., He Y., Li X., *Journal of Energy Chemistry*, **2019**, *31*, 54

[12] Dubal D. P., Gomez-Romero P., Sankapal B. R., Holze R., *Nano Energy*, **2014**, *11*, 377

[13] Yang F., Zhang K., Li W., Xu K., *Journal of Colloid and Interface Science*, **2019**, *556*, 386

[14] Deng X., Fan Y., Zhou Q., Huang H., Zhou W., Lan Z., Liang X., Li G., Guo J., Tang S., *Electrochimica Acta*, **2019**, *319*, 783

[15] Yuan C., Li J., Hou L., Zhang X., Shen L., Lou X. W.(David), *Advanced Functional Materials*, **2012**, *22*, 4592

[16] Rakhi R. B., Chen W., Cha D., Alshareef H. N., *Nano Letter*, **2012**, *12*, 2559

[17] Zhao H., Liu L., Vellacheri R., Lei Y., *Advanced Science*, **2017**, *4*, 1700188

[18] Liu C., Jiang W., Hu F., Wu X., Xue D., *Inorganic Chemistry Frontiers*, **2018**, *5*, 835

[19] Zhang Y., Wang X., Shen M., Fu X., Huang M., Liu X., Zhang Y. X., *Journal of Materials Science*, **2019**, *54*, 4821

[20] Sethi M., Bhat D. K., *Journal of Alloys and Compounds*, **2019**, *781*, 1013

[21] Zhang H., Xiao D., Li Q., Ma Y., Yuan S., Xie L., Chen C., Lu C., *Journal of Energy Chemistry*, **2017**, *27*, 195

[22] Xiao T., Li J., Zhuang X., Zhang W., Wang S., Chen X., Xiang P., Jiang L., Tan X., *Electrochimica Acta*, **2018**, *269*, 397

[23] Guan C., Liu X., Ren W., Li X., Cheng C., Wang J., *Advanced Energy Materials*, **2017**, *7*, 1602391

[24] Fu H. Y., Wang Z. Y., Li Y. H., Zhang Y. F., *Materials Research Innovations*, **2015**, *19*, S255

[25] Cheng G., Kou T., Zhang J., Si C., Gao H., Zhang Z., *Nano Energy*, **2017**, *38*, 155

[26] Cui B., Lin H., Liu Y., Li J., Sun P., Zhao X., Liu C., *Journal Physical Chemistry C*, **2009**, *113*, 14083

[27] Guo D., Zhang L., Song X., Tan L., Ma H., Jiao J., Zhu D., Li F., *New Journal of Chemistry*, **2018**, *42*, 8478

[28] Yan D., Wang W., Luo X., Chen C., Zeng Y., Zhu Z., *Chemical Engineering Journal*, **2018**, *334*, 864

[29] Shen L., Che Q., Li H., Zhang X., *Advanced Functional Materials*, **2014**, *24*, 2630

[30] Gao S., Liao F., Ma S., Zhu L., Shao M., *Journal of Materials Chemistry A*, **2015**, *3*, 16520

[31] Zhao L., Wang L., Yu P., Tian C., Feng H., Diao Z., Fu H., *Dalton Transactions*, **2017**, *46*, 4717

[32] Largeot C., Portet C., Chmiola J., Taberna P. L., Gogotsi Y., Simon P., *Journal of American Chemical Society*, **2008**, *130*, 2730

[33] Naresh B., Krishna T. N. V., Rao S. S., Kim H. J., *Materials Letters*, **2019**, *248*, 218

[34] Jabeen N., Xia Q., Yang M., Xia H., *ACS Applied Materials & Interfaces*, **2016**, *8*, 6093

[35] Ai Y., Ma J., Wang Z. M., *Earth and Environmental Science*, **2018**, *170*, 032095

[36] Yedluri A. K., Kim H., *RSC Advances*, **2019**, *9*, 1115

[37] Deng F., Yu L., Cheng G., Lin T., Sun M., Ye F., Li Y., *Journal of Power Sources*, **2014**, *251*, 202

[38] Waghmode R. B., Torane A. P., *Journal of Materials Science: Materials in Electronics*, **2016**, *27*, 6133

[39] Zhang Y., Ma M., Yang J., Su H., Huang W., Dong X., *Nanoscale*, **2014**, *6*, 4303

[40] Wang H., Wang X., Yang J., *ACS Applied Materials & Interfaces*, **2013**, *5*, 6255

[41] Xu J., Liu F., Peng X., Li J., Yang Y., Jin D., *Chemistryselect*, **2017**, *2*, 5189